
Structural changes in $\text{As}_{40}\text{S}_{60-x}\text{Se}_x$ thin films due to annealing and irradiation: Raman spectroscopy studies

¹Voynarovych I., ²Hopko M., ²Edinak O. and ^{1,2}Gomonnai A. V.

¹ Institute of Electron Physics, Ukrainian National Academy of Sciences,
21 Universytetska Street, 88017 Uzhhorod, Ukraine; e-mail: voynar@ukr.net

² Uzhhorod National University, 46 Pidhirna Street, 88000 Uzhhorod, Ukraine

Received: 18.04.2022

Abstract. We discuss evolution of Raman spectra for vitreous chalcogenide $\text{As}_{40}\text{S}_{60-x}\text{Se}_x$ ($x = 0, 20, 30, 40$ and 60 at. %) layers, which occurs under thermal annealing and irradiation with the light of different wavelengths. It is demonstrated that composition dependences of the spectral Raman intensities are consistent with existence of ‘mixed’ $\text{As}_2\text{S}_{3-x}\text{Se}_x$ pyramids. We reveal that the changes in the Raman spectra are associated with thermo- and photo-induced polymerization of the molecular fragments of mixed $\text{As}_4\text{S}(\text{Se})_4$ -type cages and $\text{S}(\text{Se})$ rings or chains.

Keywords: ternary chalcogenide As–S–Se glasses, thin films, photo-induced changes, Raman spectra.

UDC: 535.4

1. Introduction

Chalcogenide glasses and thin films are attractive owing to structural flexibility of their glass network, which results in a plethora of photo-induced changes of their physical and chemical properties [1–5]. As a consequence, chalcogenide glasses represent promising materials for integrated optics/photonics. The appropriate examples involve photo- and electron resists, sensors [5, 6], optical storage and memory devices [7], and all-optical processing [8] (e. g., micro-structured optical fibres [9] and holographic gratings [10]).

Better understanding of the structural properties of those materials can aid in optimizing construction and sensitivity of nanocrystalline composites based on binary (As–S(Se)) or ternary (As–S–Se) chalcogenide glasses. This is especially important since the latter glasses can be applied for direct recording of optical elements. Note that, in most of the previous works, studies of the changes occurring in optical, structural and surface properties of chalcogenide-glass thin films [11–14] and glasses [15] have been performed using c. w. Ar^+ , He–Ne or He–Cd lasers with the light wavelengths $\lambda = 514.5, 632.8$ and 440 nm, respectively.

Raman spectroscopy has been widely used for studying the structure of the above binary and ternary chalcogenide glasses and the thin films on their basis and analyzing the photo-induced effect in those materials [16, 17]. As example, the authors [17] have elucidated the changes in their optical absorption, bandgap energy, refraction index and kinetic parameters, which take place under irradiation with both narrow-band and wide-band light corresponding to the photon energies that range from over- to under-bandgap ones. Nonetheless, Raman spectra needed for characterizing the origin of structural changes associated with annealing and irradiation with different light wavelengths have not yet been analyzed.

In the present work, we employ the Raman spectroscopy to characterize the structural changes in as-evaporated films of the ternary As–S–Se glasses corresponding to the whole

stoichiometric row ($\text{As}_{40}\text{S}_{60}\text{--As}_{40}\text{Se}_{60}$). These are the changes occurring under annealing and irradiation with different LEDs (the wavelengths $\lambda_{\text{max}} = 375\text{--}740\text{ nm}$).

2. Experimental

Bulk amorphous chalcogenide glasses $\text{As}_{40}\text{S}_{60-x}\text{Se}_x$ (with $x = 0, 20, 30, 40$ and 60) were prepared from high-pure (99.999%) precursor elements, using a conventional melt-quenching technique and evacuated quartz ampoules. The glasses were synthesized in a frequently rocked furnace at 500°C during 24 h. After that they were heated up to 850°C for successful homogenization. Thin films of the above glasses were prepared by thermal evaporation from a tantalum cell onto silicate glass substrates kept at the room temperature (the rate $1\text{--}2\text{ nm s}^{-1}$). The evaporation rate and the thickness of the thin films were controlled using a monitoring system based upon crystalline quartz.

The thicknesses of as-evaporated thin films were equal to $1\text{ }\mu\text{m}$. As-deposited films were annealed in the air (the temperature 160°C and the time duration 12 h). These films were exposed to radiation of Roither Lasertechnik LEDs (Austria), with the maximum output emission power of 100 mW/cm^2 . The corresponding wavelengths were equal to 375, 405, 450, 525, 630, 690 and 740 nm, while the exposure times amounted up to 60 min for each thin film. The thin films of different compositions were irradiated with the LEDs of which photon energies corresponded to over-bandgap (405 nm), bandgap and under-bandgap light (see Table 1). Notice that the bandgap energies for all the compounds were taken from Ref. [17].

Table 1. Some optical parameters of as-deposited $\text{As}_{40}\text{S}_{60-x}\text{Se}_x$ thin films, and wavelengths of LEDs used for their irradiation.

x , at. %	E_g^{opt} , eV	λ_{bandgap} , nm	λ_{LED} (over-bandgap), nm	λ_{LED} (bandgap), nm	λ_{LED} (under-bandgap), nm
0	2.394	518	405	450	570
20	2.143	578	405	525	690
30	2.035	609	405	525	690
40	1.940	639	405	570	740
60	1.788	693	405	690	790

The Raman spectra of bulk $\text{As}_{40}\text{S}_{60-x}\text{Se}_x$ glasses and corresponding thin films were measured at the room temperature in the spectral range from 100 to 550 cm^{-1} . Our IFS 55 (Bruker) FTIR spectrometer was equipped by an FRA 106 Raman spectroscopy module that worked with a Nd:YAG laser (1064 nm) as excitation source.

The Raman spectra were normalized by the integrated spectral intensity and analyzed using Fityk software [18] for data processing and multiple-peak fitting. To resolve overlapping lines in the complex Raman spectra of our ternary As–Se–S compounds, we used an approximation of Voigt profiles, i.e. a convolution of Gaussian and Lorentzian functions.

3. Results and discussion

The Raman spectra obtained for the bulk glasses, the thermally evaporated films and the annealed films of $\text{As}_{40}\text{S}_{60-x}\text{Se}_x$ are presented in Fig. 1. As seen from Fig. 1, all the spectra detected for the sulphur- and selenium-containing bulk glasses and the appropriate thin films reveal two principal bands. One of these is located between 200 and 280 cm^{-1} and the other between 300 and 400 cm^{-1} , which is similar to the data reported earlier in Refs. [19–22]. The bands observed in the region of primary maximum for the bulk $\text{As}_{40}\text{S}_{60}$ glass ($300\text{--}400\text{ cm}^{-1}$) can be attributed to the stretching mode of As–S bonds of $\text{AsS}_{3/2}$ pyramidal units or As_4S_4 cages (362 cm^{-1}) and the vibrations of $\text{AsS}_{3/2}$

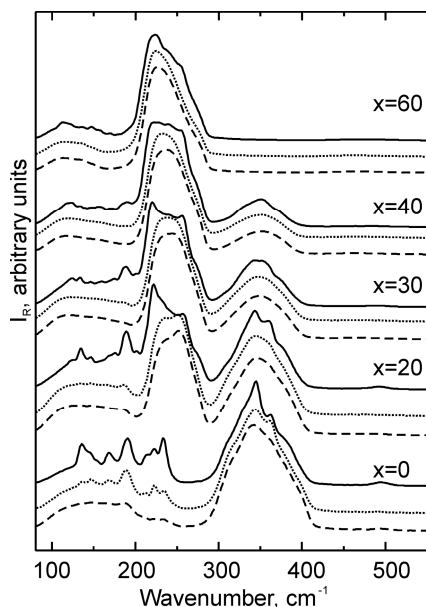


Fig. 1. Raman spectra detected for the bulk glass (dashed lines) and the as-evaporated (solid lines) and annealed (dotted lines) thin films of ternary $\text{As}_{40}\text{S}_{60-x}\text{Se}_x$ compounds.

vibrations of the Se–Se bonds in Se_n chains [19]. Note that a number of specific features also appear in the region $100\text{--}200\text{ cm}^{-1}$ of the Raman spectra, which have also been obtained for As-rich glasses of the As–Se system [36]. Similar features have also been found in the films and glasses of the As–S system [5, 7, 19]. They are mainly treated as the As–As and S–S vibrations that occur in molecular As_4S_4 fragments.

Thermally evaporated thin films of the stoichiometric $\text{As}_{40}\text{Se}_{60}$ glasses often contain some of molecular species, of which vapour is composed due to thermal dissociation of the bulk glass. For $\text{As}_{40}\text{S}_{60}$, As_4S_4 and S_2 units dominate in the vapour [27] and many molecular fragments (e.g., As, As_4 , S_2 , As_4S_4 and As_4S_3) are present during film deposition [27, 28]. The mass spectra of the vapour above As_2Se_3 reveal a considerable number of As_4 , As_3Se , As_2Se_2 , Se_2 and As_4Se_3 molecules [29]. Since these compounds are of molecular type, they should be dissolved in a three-dimensional glass as molecular or nanosized particles. Thus, the features seen in the Raman spectra of the as-evaporated $\text{As}_{40}\text{S}_{60}$ and $\text{As}_{40}\text{Se}_{60}$ thin films (see Fig. 1) are narrower because of their molecular nature [4, 19, 22].

According to the results reported earlier [28], chaotic replacement of chalcogens of one type by chalcogens of another type can occur in the network

pyramidal units (the shoulders occurring at 310 , 331 and 380 cm^{-1}) [23, 33–35]. A weak broad band observed at 495 cm^{-1} is associated with the S–S stretching vibration in S_8 rings and chains. There are numerous weak bands located at 135 , 145 , 154 , 168 , 190 , 212 , 222 and 231 cm^{-1} in the region $90\text{--}200\text{ cm}^{-1}$ of the Raman spectra detected for arsenic sulphide. They can be attributed to the As–As bonds of As_4S_4 cages [23].

The strongest band in the spectrum of bulk $\text{As}_{40}\text{Se}_{60}$ glass (227 cm^{-1}) is attributed to $\text{AsSe}_{3/2}$ pyramidal units [1, 28, 29, 32]. In the higher-frequency region, the band located at 241 cm^{-1} can be assigned to Se_n chains and/or As_4Se_4 structural units [19, 31]. The band 254 cm^{-1} corresponds to the Se–Se vibrations in Se_n rings [19, 32, 33], whereas the band 273 cm^{-1} can be assigned to the Se–Se bonds in AsSe_3 pyramidal units and As_4Se_4 (As_4Se_3) cages [31]. The broad band detected at $440\text{--}480\text{ cm}^{-1}$ (see Fig. 4) should be related to

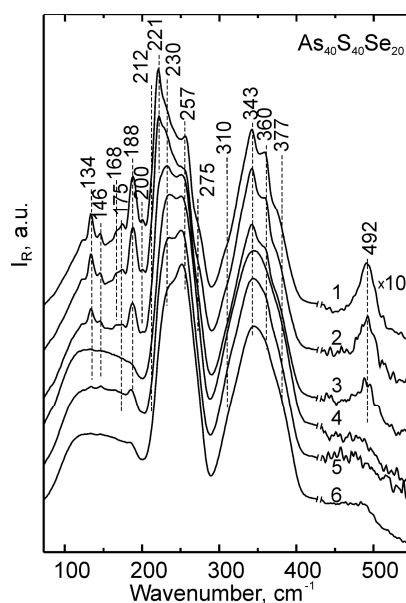


Fig. 2. Raman spectra detected for the bulk ternary $\text{As}_{40}\text{S}_{40}\text{Se}_{20}$ compound (curve 6), its as-deposited (curve 1) and annealed (curve 5) thin films and the films irradiated with the bandgap (curve 4, $\lambda_{\text{LED}} = 525\text{ nm}$), under-bandgap (curve 2, $\lambda_{\text{LED}} = 690\text{ nm}$) and over-bandgap (curve 3, $\lambda_{\text{LED}} = 405\text{ nm}$) light.

structure of the bulk ternary As–S–Se glasses. Then the network of these glasses consists mainly of AsS_3 , AsSe_3 , AsSSe_2 and As_2Se_3 pyramids. The structure of the as-evaporated $\text{As}_{40}\text{S}_{60-x}\text{Se}_x$ thin films should also contain mixed pyramidal structural units $\text{AsS}_{3-n}\text{Se}_n$ ($n = 0, 1, 2$ and 3) and a significant number of defects, such as mixed molecular species $\text{As}_4\text{S}(\text{Se})_4$ and $\text{As}_4\text{S}(\text{Se})_3$, and $\text{S}(\text{Se})_n$ rings and chains. According to Ref. [28], the Raman spectra of our glasses and films containing these mixed structural units do not reveal new bands (see Fig. 2 to Fig. 4), if compared with the stoichiometric As_2S_3 or As_2Se_3 glasses. Only evolution of the Raman bands is observed with changing composition.

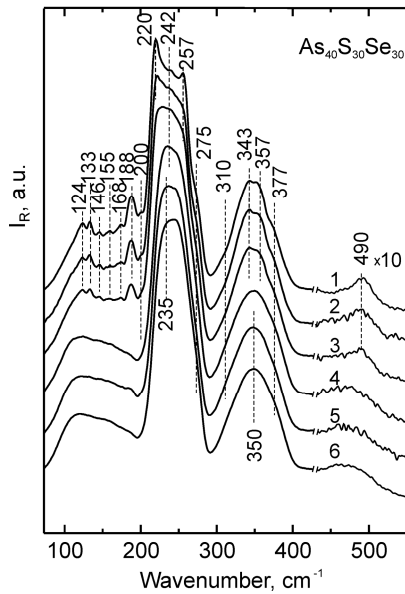


Fig. 3. Raman spectra detected for the bulk ternary $\text{As}_{40}\text{S}_{30}\text{Se}_{30}$ compound (curve 6), its as-deposited (curve 1) and annealed (curve 5) thin films and the films irradiated with the bandgap (curve 4, $\lambda_{\text{LED}} = 525$ nm), under-bandgap (curve 2, $\lambda_{\text{LED}} = 690$ nm) and over-bandgap (curve 3, $\lambda_{\text{LED}} = 405$ nm) light.

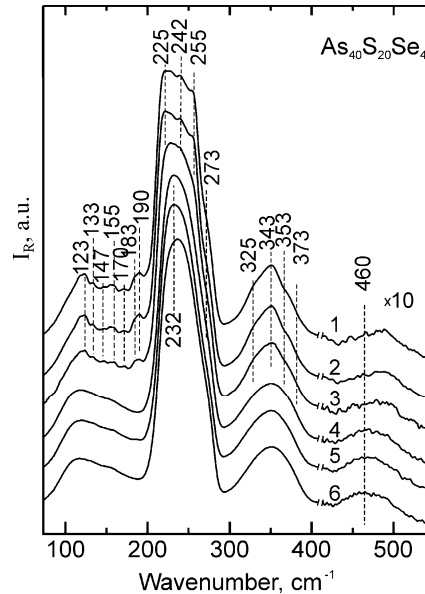


Fig. 4. Raman spectra detected for the bulk ternary $\text{As}_{40}\text{S}_{20}\text{Se}_{40}$ compound (curve 6), its as-deposited (curve 1) and annealed (curve 5) thin films and the films irradiated with the bandgap (curve 4, $\lambda_{\text{LED}} = 570$ nm), under-bandgap (curve 2, $\lambda_{\text{LED}} = 740$ nm) and over-bandgap (curve 3, $\lambda_{\text{LED}} = 405$ nm) light.

Numerous weak bands detected in the region $90\text{--}200\text{ cm}^{-1}$ and the band located near 495 cm^{-1} (see Fig. 2 to Fig. 4) can be associated with ‘wrong’ homopolar As–As and S–S bonds in these mixed non-stoichiometric structural units. The band 254 cm^{-1} can be assigned to Se_8 -ring vibrations, while the band 240 cm^{-1} can be formed by overlapping the vibrations of Se_n chains with those of $\text{As}_4(\text{S})\text{Se}_3$ molecules. Contrary to the band located at 205 cm^{-1} in the Raman spectra of as-deposited $\text{As}_{40}\text{Se}_{60}$, which is attributed to the vibrations of structural As_4Se_4 units, the band 220 cm^{-1} is clearly detected in the spectra of the as-deposited thin films with the ternary composition (see Fig. 5). It can be attributed to the mixed $\text{As}_4(\text{S}_{1-n}\text{Se}_n)_4$ structure. The band 275 cm^{-1} , which appears only as a shoulder, is well visible in the spectra of As_4Se_3 thin film. It seems to be due to the presence of –Se–Se–bridges between pyramidal $\text{AsS}_{3-n}\text{Se}_n$ units and/or $\text{As}_4(\text{S}_{1-n}\text{Se}_n)_4$ cages.

The principal bands detected in the regions $200\text{--}280\text{ cm}^{-1}$ and $300\text{--}400\text{ cm}^{-1}$ in all of the Raman spectra measured by us have been fitted using a series of Voigt peaks. As an example for $\text{As}_{40}\text{S}_{30}\text{Se}_{30}$ compound, Fig. 5 shows the Voigt decomposition of the Raman spectra obtained for the bulk glass, the virgin thin film and the film irradiated with the bandgap light. The vibration frequencies of the known structural units of As_2Se_3 and As_2S_3 glasses reported in the literature

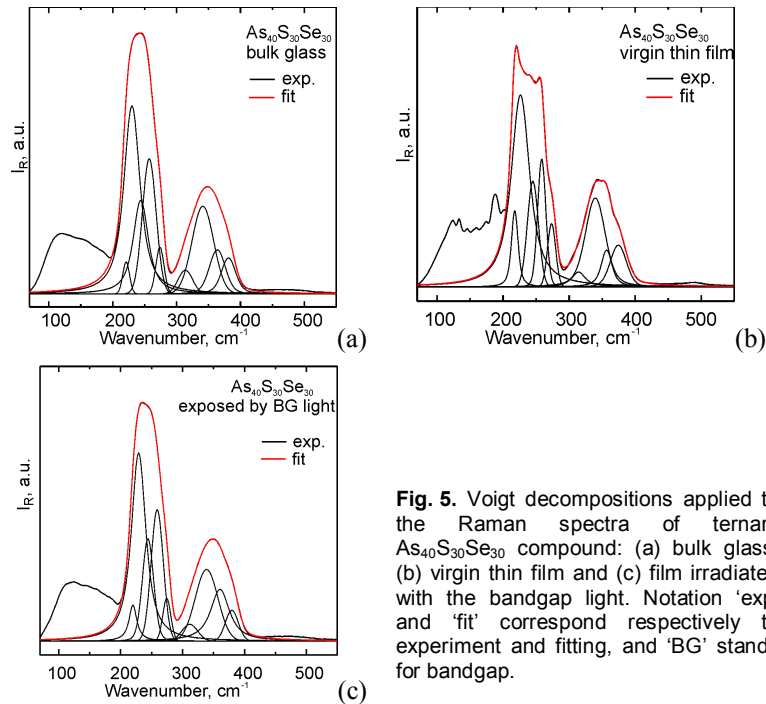


Fig. 5. Voigt decompositions applied to the Raman spectra of ternary $\text{As}_{40}\text{S}_{30}\text{Se}_{30}$ compound: (a) bulk glass, (b) virgin thin film and (c) film irradiated with the bandgap light. Notation ‘exp’ and ‘fit’ correspond respectively to experiment and fitting, and ‘BG’ stands for bandgap.

[21–26] have been used as initial parameters for the Voigt decomposition. The experimental data has been fitted using the width and height variation. While fitting the Raman spectra, the deviation of peak positions up to 2 cm^{-1} has been allowed.

The compositional dependence of the positions of peak maxima has been derived using the same Voigt decomposition of the Raman spectra (see Fig. 6 to Fig. 8). As seen from Fig. 6 and Fig. 7, the positions of the band maxima located near 380 , 362 and 345 cm^{-1} are shifted toward lower photon frequencies with increasing Se content in the ternary As–S–Se compounds. Increasing Se content slightly shifts the position of the maximum near 310 cm^{-1} toward higher frequencies. In the region $200\text{--}280\text{ cm}^{-1}$ (see Fig. 8), only the bands 227 and 220 cm^{-1} attributed respectively to pyramidal $\text{AsSe}_{3/2}$ and As_4Se_4 units move slightly toward higher frequencies with decreasing Se content. This shift should be expected in a mixed crystalline system revealing a ‘two-mode’ behaviour, similar to the situation reported for $\text{CdS}_x\text{Se}_{1-x}$ alloys [30].

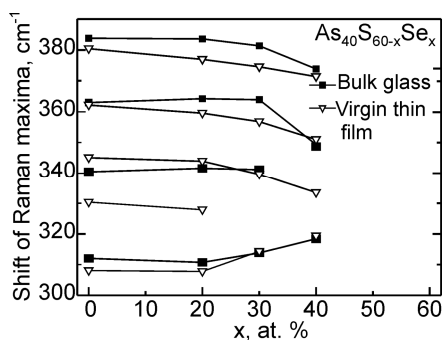


Fig. 6. Shifts in band maximums detected for the Raman spectra of the bulk glass and the virgin thin films of ternary $\text{As}_{40}\text{S}_{60-x}\text{Se}_x$ compounds. Lines are only guides for the eye.

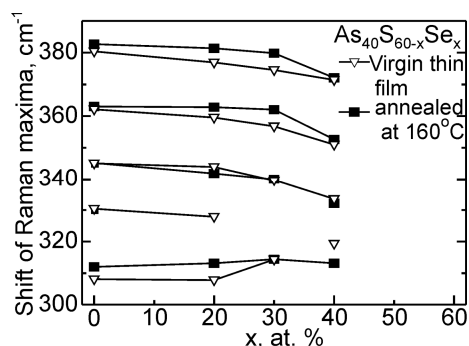


Fig. 7. Shifts in band maximums detected for the Raman spectra of the virgin and annealed thin films of ternary $\text{As}_{40}\text{S}_{60-x}\text{Se}_x$ compounds. Lines are only guides for the eye.

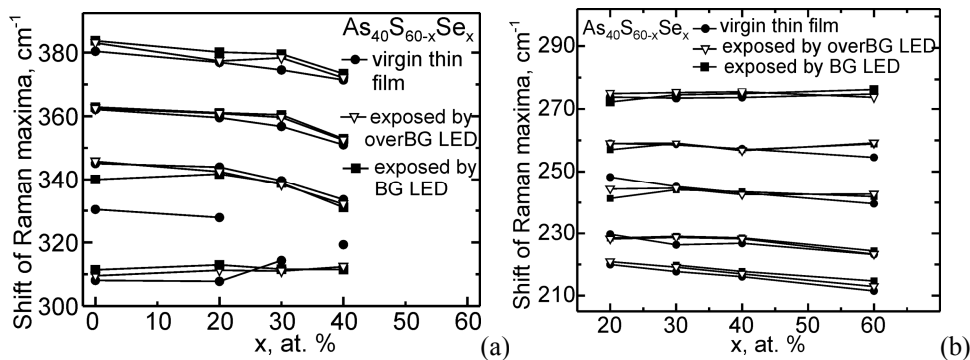


Fig. 8. Shifts in band maxima detected for the Raman spectra of the as-evaporated thin films of ternary $\text{As}_{40}\text{S}_{60-x}\text{Se}_x$ compounds and the films irradiated with the over-bandgap and bandgap light: panels (a) and (b) refer to the broad bands located respectively near 250 and 360 cm^{-1} . Lines are only guides for the eye and 'BG' stands for bandgap.

As seen from Fig. 2 to Fig. 4, the changes in the Raman spectra taking place due to annealing and irradiation by the bandgap light are very similar to each other. All of the narrow bands located in the region 100–200 cm^{-1} , which are mainly associated with the 'wrong' As–As homopolar bonds in $\text{As}_4(\text{S}_{3-n}\text{Se}_n)_4$ and $\text{As}_4(\text{S}_{3-n}\text{Se}_n)_3$ molecules, decrease in their intensity. In the region 220–280 cm^{-1} where the dominant bands of As–Se system appear, both the annealing and the irradiation by the bandgap light cause transformation of the narrow Raman bands related to molecular As_4Se_4 and As_4Se_3 fragments, Se_8 rings and Se_n chains (located respectively at 220, 255 and 270 cm^{-1}) into the broad band positioned near 227 cm^{-1} (see Fig. 2 to Fig. 4). The latter band is associated with the stretching vibration modes of pyramidal AsSe_3 units.

The same behaviour was found in the regions 300–380 and 400–550 cm^{-1} . The annealing and the irradiation by the bandgap light decrease the intensity of the shoulders located at 310, 362 and 380 cm^{-1} , which are related to the As–As bonds in As_4S_4 cages. The weak broad bands observed at 495 and 440–480 cm^{-1} , which are attributed respectively to the S–S and Se–Se bonds in $\text{S}(\text{Se})_n$ chains, totally disappear due to the thermal annealing and the irradiation. A decrease in the role of 'wrong' bonds indicates transformation of the mentioned molecular species into the binary ($\text{AsS}_{3/2}$ and $\text{AsSe}_{3/2}$) and mixed ($\text{AsS}_{3-n}\text{Se}_n$, with $n = 0, 1, 2$ and 3) pyramidal structural units of chalcogenide-glass network. In other words, here we deal with a thermo- or photo-induced chemical reactions [1].

Irradiation by the over- and under-bandgap light only slightly decreases the intensity of all the narrow bands located in the region 100–200 cm^{-1} and the narrow shoulders found at 220–280 cm^{-1} and 300–380 cm^{-1} (see curves 2 and 3 in Fig. 2 to Fig. 4). Such behaviour can be ascribed to a small penetration depth peculiar for the over-bandgap light. For a 1- μm thin film of ternary As–S–Se system, the penetration depth of the radiation of 405-nm LED amounts to 100–200 nm. Obviously, the photo-induced chemical reactions can take place only within this narrow near-surface region of the thin film. On the contrary, the absorption of the under-bandgap light is quite low. Then the light is not absorbed and so it cannot transfer any energy to the material in order to induce structural changes.

5. Conclusion

In this work we have experimentally studied and interpreted the changes in the structure of amorphous ternary $\text{As}_{40}\text{S}_{60-x}\text{Se}_x$ thin films ($x = 0, 20, 30, 40$ and 60 at. %), which occur under thermal annealing and irradiation with the light of different wavelengths. Both the thermal

annealing and the irradiation with the bandgap and over-bandgap light lead to partial thermo- and photo-induced polymerization of molecular structural units into a continuous network, which is characteristic for the bulk glasses with appropriate stoichiometric compositions. The shifts of the Raman bands that take place with varying $\text{As}_{40}\text{S}_{60-x}\text{Se}_x$ composition reveal a clear ‘two-mode’ behaviour.

References

1. Kolobov A and Tominaga J. Chalcogenides: metastability and phase change phenomena. Berlin: Springer, 2012.
2. Yannopoulos S. Photo-plastic effects in chalcogenide glasses: Raman scattering studies. In: Kolobov A (Ed.), Photo-Induced Metastability in Amorphous Semiconductors. Weinheim: Wiley-VCH, 2003.
3. Frumar M, Frumarová B, Wágner T and Němec P. Photo-induced phenomena in amorphous and glassy chalcogenides. In: Kolobov A V (Ed.), Photo-Induced Metastability in Amorphous Semiconductors. Weinheim: Wiley-VCH, 2003.
4. Wang F and Boolchand P. Photostructural transformations and global connectedness of network glasses. In: Lucovsky G and Popescu M (Eds.), Non-Crystalline Materials for Optoelectronics. Bucharest: INOE, 2004.
5. Tanaka K and Shimakawa K. Amorphous chalcogenide semiconductors and related materials. Berlin: Springer, 2011.
6. Shpotyuk O, 1995. Amorphous chalcogenide semiconductors for dosimetry of high-energy ionizing radiation. *Rad. Phys. Chem.* **46**: 1279–1282.
7. Wutting M and Yamada N, 2007. Phase-change materials for rewriteable data storage. *Nature Mater.* **6**: 824–832.
8. Laniel J M, Ho N, Vallee R and Villeneuve A J, 2005. Nonlinear-refractive-index measurement in As_2S_3 channel waveguides by asymmetric self-phase modulation. *J. Opt. Soc. Amer. B.* **22**: 437–445.
9. Toupin P, Brilland L, Renversez G and Troles J, 2013. All-solid all-chalcogenide microstructured optical fiber. *Opt. Express.* **21**: 14643–14648.
10. Ahmad R, Rochette M and Baker Ch, 2011. Fabrication of Bragg gratings in subwavelength diameter As_2Se_3 chalcogenide wires. *Opt. Lett.* **36**: 2886–2888.
11. Azhniuk Y M, Dzhagan V M, Solonenko D, Mukherjee A, Loya V Y, Grytsyshche I V, Lopushansky V V, Gomonnai A V and Zahn D R T, 2019. Laser annealing-induced formation of CdS nanocrystals in Cd-doped amorphous As_2S_3 thin films. *Phys. Stat. Sol. B.* **256**: 1800298.
12. Azhniuk Y M, Solonenko D, Loya V Y, Kryshenik V M, Lopushansky V V, Mukherjee A, Gomonnai A V and Zahn D R T, 2019. Flexoelectric and local heating effects on CdSe nanocrystals in amorphous As_2Se_3 films. *Mater. Res. Express.* **6**: 095913.
13. Azhniuk Y M, Solonenko D, Sheremet E, Dzhagan V M, Loya V Y, Grytsyshche I V, Schulze S, Hietschold M, Gomonnai A V and Zahn D R T, 2019. Structural and optical study of Zn doped As_2Se_3 thin films: Evidence for photoinduced formation of ZnSe nanocrystallites. *AIP Adv.* **9**: 065212.
14. Azhniuk Y, Dzhagan V, Solonenko D, Loya V, Grytsyshche I, Lopushansky V V, Gomonnai A V and Zahn D R T, 2019. In-doped As_2Se_3 thin films studied by Raman and X-ray photoelectron spectroscopies. *Appl. Surf. Sci.* **471**: 943–949.
15. Azhniuk Y M, Stoyka V, Petryshynets I, Rubish V M, Guranich O G, Gomonnai A V, Zahn D

-
- R T, 2012. SbSI nanocrystal formation in As–Sb–S–I glass under laser beam. *Mater. Res. Bull.* **47**: 1520–1522.
16. Kozdras A, Golovchak R, Shpotyuk O and Szymura S, 2011. Light-assisted physical aging in chalcogenide glasses: Dependence on the wavelength of incident photons. *J. Mater. Res.* **26**: 2420–2427.
 17. Voynarovych I, Buzek J, Palka K and Vlček M, 2016. Spectral dependence of photoinduced optical effects in $\text{As}_{40}\text{S}_{60-x}\text{Se}_x$ thin films. *Thin Sol. Films.* **608**: 8–15.
 18. Wojdyr M, 2010. Fityk: a general-purpose peak fitting program. *J. Appl. Cryst.* **43**: 1126–1128.
 19. Solin S A and Papatheodorou G N, 1977. Irreversible thermostructural transformations in amorphous As_2S_3 films: a light-scattering study. *Phys. Rev. B.* **15**: 2084–2090.
 20. Shpotyuk O I, Kasperczyk J and Kityk I V, 1997. Mechanism of reversible photoinduced optical effects in amorphous As_2S_3 . *J. Non-Cryst. Sol.* **215**: 218–225.
 21. Nemanich R J, Connel G A N, Hayers T M and Street R A, 1978. Thermally induced effects in evaporated chalcogenide films. *Phys. Rev. B.* **18**: 6900–6914.
 22. Shpotyuk O I, 2003. On the microstructural origin of reversible photo-induced transformations in amorphous As_2Se_3 . *Opto-Electron. Rev.* **11**: 19–25.
 23. Frumar M, Polák Z and Černošek Z, 1999. Raman spectra and photostructural changes in the short-range order of amorphous As–S chalcogenides. *J. Non-Cryst Sol.* **256&257**: 105–110.
 24. Wagner T, Kasap S O, Vlček M, Sklenar A and Stronski A V, 1998. The structure of $\text{As}_x\text{S}_{100-x}$ glasses studied by modulated temperature differential scanning calorimetry and Raman spectroscopy. *J. Non-Cryst. Sol.* **227–230**: 752–756.
 25. Golovchak R, Shpotyuk O, McCloy J S, Riley B J, Windisch C F, Sundaram S R, Kovalskiy A and Jain H, 2010. Structural model of homogeneous As–S glasses derived from Raman spectroscopy and high-resolution XPS. *Phil. Mag.* **90**: 4489–4501.
 26. Liska M, Chromcikova M, Holubova Y and Cernosek Z, 2014. Thermodynamic model and structure of As_2S_3 - As_2Se_3 glasses based on the MCR analysis of Raman spectra. *Ceramics.* **58**: 95–98.
 27. Tanaka K, 1980. Optical properties and photoinduced changes in amorphous As–S films. *Thin Sol. Films.* **66**: 271–279.
 28. Freitas J A, Strom U and Treacy D J, 1983. Raman scattering of the mixed chalcogenide glass system $\text{As}_2\text{S}_x\text{Se}_{3-x}$. *J. Non-Cryst. Solids.* **59&60**: 875–878.
 29. Stronski A V, Vlček M and Olesenko P F, 2001. Fourier Raman spectroscopy studies of the $\text{As}_{40}\text{S}_{60-x}\text{Se}_x$ glasses. *Semicond. Phys., Quant. Electron. & Optoelectron.* **4**: 210–213.
 30. Chang I F and Mitra S S, 1968. Application of a modified random-element-isodisplacement model to long-wavelength optic phonons of mixed crystals. *Phys. Rev.* **172**: 924–933.
 31. Iovu M S, Kamitsos E I, Varsamis C P E, Boolchand P and Popescu M, 2005. Raman spectra of $\text{As}_x\text{Se}_{100-x}$ and $\text{As}_{40}\text{Se}_{60}$ glasses doped with metals. *Chalcogenide Lett.* **2**: 21–26.
 32. Li W, Seal S, Rivero C, Lopez C, Richardson K, Pope A, Schulte A, Myneni S, Jain H, Antoine K and Miller A C, 2005. Role of S/Se ratio in chemical bonding of As–S–Se glasses investigated by Raman, X-ray photoelectron, and extended X-ray absorption fine structure spectroscopies. *J. Appl. Phys.* **98**: 053503.
 33. Stronski A V, Vlček M, Kostyukevych S A, Tomchuk V M and Kostyukevych E V, 2002. Study of non-reversible photostructural transformations in $\text{As}_{40}\text{S}_{60-x}\text{Se}_x$ layers applied for fabrication of holographic protective elements. *Semicond. Phys., Quant. Electron. & Optoelectron.* **5**: 284–287.
 34. Messaddeq S H, Boily O, Santagneli S H, El-Amraoui M and Messaddeq Y, 2016. As_4S_4 role on the photoinduced birefringence of silver-doped chalcogenide thin films. *Opt. Mater.*

6:1452–1463.

35. Wagner T, Perina V, Mackova A, Rauhala E, Seppala A, Vlček Mir, Karap S O, Vlček Mil and Frumar M, 2001. The tailoring of the composition of Ag–As–S amorphous films using photo-induced solid state reaction between Ag and $As_{30}S_{70}$ films. *Solid State Ionics*. **141–142**: 387–395.
36. Kovanda V, Vlček Mir and Jain H, 2003. Structure of As–Se and As–P–Se glasses studied by Raman spectroscopy. *J. Non-Cryst. Sol.* **326–327**: 88–92.

Voynarovych I., Hopko M., Edinak O. and Gomonnai A. V. 2022 Structural changes in $As_{40}S_{60-x}Se_x$ thin films due to annealing and irradiation: Raman spectroscopy studies. *Ukr.J.Phys.Opt.* **23**: 133 – 141. doi: 10.3116/16091833/23/3/133/2022

***Анотація.** Обговорено еволюцію спектрів комбінаційного розсіяння для склоподібних шарів халькогенідів $As_{40}S_{60-x}Se_x$ ($x = 0, 20, 30, 40$ і 60 ат. %), яка відбувається при термічному відпалі та опроміненні світлом різних довжин хвиль. Показано, що композиційні залежності спектральних інтенсивностей комбінаційного розсіяння узгоджуються з існуванням «змішаних» пірамід $As_2S_{3-x}Se_x$. Виявлено, що зміни в спектрах комбінаційного розсіяння пов'язані з термо- та фотоіндукованою полімеризацією молекулярних фрагментів змішаних структурних клітинок типу $As_4S(Se)_4$ і кілець або ланцюгів $S(Se)$.*